ELSEVIER

Fluid Dynamics Research 27 (2000) 183–197

FLUID DYNAMICS RESEARCH

Flow visualization study of role of coherent structures in a tab wake

R. Elavarasan [1], Hui Meng *

Department of Mechanical and Nuclear Engineering, Kansas State University, Manhattan, KS 66506, USA

Received 3 August 1998; received in revised form 2 June 1999; accepted 4 December 1999

Abstract

A simple surface-mounted tapered tab has recently attracted fluids research both for its ability to enhance mixing and heat transfer (for which it is known as high-efficiency vortab mixer) and for its generation of coherent structures that are topologically similar to those found in natural turbulent boundary layers. Two types of structures, namely pressure-driven counter-rotating vortex pair (CVP) and hairpin vortices were previously identified in the tab wake, but the contribution of individual structures to the mixing enhancement process and how they interact are not known. In the present study, flow visualization using a planar laser-induced fluorescence (PLIF) technique is carried out to probe into the flow dynamics in the wake of the mixing tab. By injecting dye at an appropriate location and illuminating the flow in various planes, the structures are visualized clearly. The results show, in contrary to earlier observations, that the two types of structures dominate different regions. At the Reynolds number of 700 based on tab height (h), the CVP has more influence in the region $0 < x/h < 1.5$. The counter-rotating action of the vortex pair induces a pumping action along the symmetry by which the low-speed fluid from the boundary layer is transported to the high-speed outer shear layer. The displaced fluid is entrained by the recirculating counter-rotating vortices and is mixed well while convecting downstream. Beyond this region, fully developed hairpin structures contribute more to mixing in a similar way as in a turbulent boundary layer. It is observed that the shedding frequency of hairpin vortices is slightly higher than the pumping frequency of the counter-rotating vortex pair. It is also observed that the hairpin structures loses their identity beyond $x/h > 15$, and there is no large-scale cross-stream mixing visible in this region.

1. Introduction

The origin of boundary layer turbulence and how it dissipates has been the objective of much research conducted in the last few decades. The identification of coherent structures in turbulent

* Corresponding author. Current address: SUNY at Buffalo, Mechanical & Aerospace Engineering Dept., Buffalo, NY 14260-4400, USA.

E-mail address: huimeng@eng.buffalo.edu (H. Meng)

[1] Current address: Dept. of Mechanical Engineering, Florida State University, Tallahassee, FL 32310, USA.

0169-5983/00/$20.00

PII: S0169-5983(00)00003-4

flows is considered one of the major advances in understanding this problem. These structures can be defined as confined regions in space and time in which a definite phase relationship exists among flow variables (such as u', v', w' and pressure). The existence of coherent structures has been established in almost all turbulent flows including near-wall turbulence.

Early experiments (Kline and Runstadler 1959; Runstadler et al., 1963) confirmed the streaky sub-layer structures in a turbulent boundary layer originally reported by Hama et al. (1957). Later Kline et al. (1967) showed that an alternating array of high- and low-speed streamwise regions in the sub-layer, called low-speed streaks, appear at random locations and times. These streaks interact with the outer layer through a process called bursting. Most of the mass, heat and momentum transfer appears to take place by this process (Corino and Brodkey, 1969; Kim et al., 1971). Later Smith and Schwartz (1983) and Smith and Metzler (1983), from flow visualization at different viewing angles, observed that the low-speed streaks are associated with counter-rotating streamwise structures which are basically formed by three-dimensional deformation and roll-up of vortices in the boundary layer. Theodorsen (1952) was one of the earlier researchers who identified the presence of these kinds of structures, which were later named "hairpin or horseshoe" vortices. Head and Bandyopadhyay (1981) carried out extensive flow visualization in the turbulent boundary layer. Their investigation revealed that the boundary layer is filled with a forest of hairpin like-structures, which are inclined along the flow direction, extending to a substantial part of the boundary layer. Nishioka et al. (1981) and Nishioka and Asai (1984) studied the evolution and role of these hairpin structures in maintaining the turbulence and momentum transfer in the wall region in detail. While studying the turbulence transition they observed that the breakdown of high-speed layer results in hairpin structures which convect downstream with a velocity of $0.6U$ (U is the free stream velocity), producing low-speed streak on their passage. Their experiment also revealed that the hairpins and associated low-speed streaks are solely responsible for wall turbulence and momentum transfer in the boundary layer. Each hairpin structure, as it leaves the surface, gives rise to a condition that favors the production of further hairpins. This process is continual such that the turbulent boundary layer is self-sustaining in absence of strong stabilizing effects (Asai and Nishioka, 1995; Panton, 1999). The studies also indicate that the hairpin structures are responsible for production of turbulent kinetic energy and Reynolds stresses in the flow and play a major role in the dynamics of the near-wall turbulence. An impressive amount of information has been collected on the kinematics of coherent structures in the turbulent boundary layer by various researchers (see Robinson, 1991 for a review).

Research has also been carried out to study the evolution and generation process of these structures by generating them artificially (Acalar and Smith, 1987a, b). The interaction of these structures with the near wall as well as outer layer fluid is observed to be responsible for mass, momentum, energy and heat transfer in the boundary layer (Peridier et al., 1991; Smith et al., 1991). As a result of this interaction the low-speed boundary layer fluid is effectively transferred to the outer layer thus increasing the local mixing. The experimental observations suggest that, by synthesizing these coherent structures in much larger scale, it should be possible to increase the mixing efficiency considerably. Based on this consideration, various vortex generators have been designed either to enhance mixing in various applications (Gretta, 1990; Harnby et al., 1985 for a collection of articles on the mixing process) or to control turbulent boundary layers (Stevens and Collins, 1955; Lin and Howard, 1989). Lately the chemical process industries are adopting various vortex generators to improve fluid mixing.

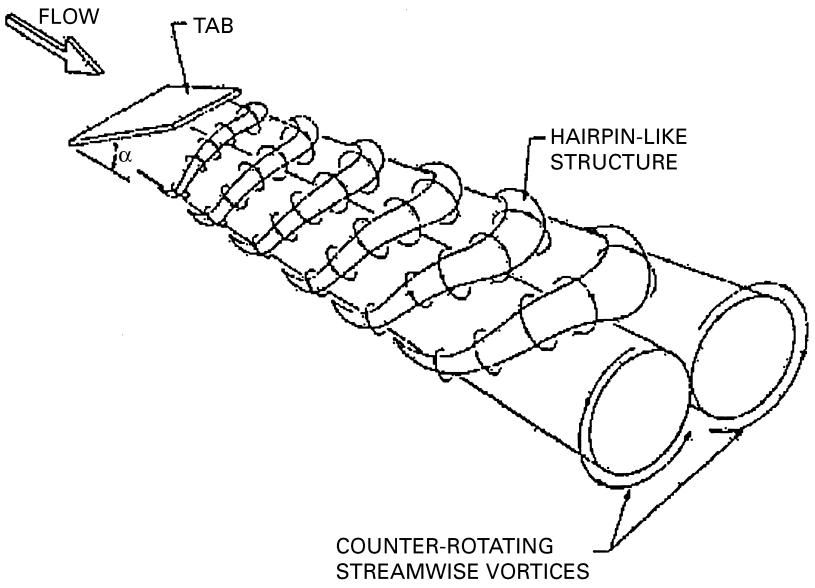

Fig. 1. Conceptual model of flow structures illustrated by Gretta and Smith (1993) in the wake of a passive mixing tab.

Along this line of research, Gretta (1990) studied various geometries of a simple mixing device consisting of a symmetrically tapered tab. By simply mounting these devices on the channel wall, large-scale structures are created in its wake resulting in considerable increase in mixing. This device is known as High Efficiency Vortab (HEV) mixer. This passive surface mixing device has proven to be very effective in enhancing the cross-stream mixing (Gretta, 1990). Owing to its performance as an efficient mixer with low pressure drop, the HEV mixer is now used in the process industries.

Apart from its mixing application, the flow behind the passive mixing device has fundamental significance, as the large-scale structures found in its wake bear topological similarity to those observed in natural turbulent boundary layers. Gretta and Smith (1993) used flow visualization and thermal anemometers to study these structures and observed that the tab shed a series of large-scale hairpin structures from its tip with sizes comparable to the height of the tab, along with a counter-rotating vortex pair (CVP) induced by pressure difference before and after the tab. They proposed a conceptual model of these structures shown in Fig. 1. These large-scale structures induced cross-stream mixing of mass and momentum in a similar way as their counterparts in a natural turbulent boundary layer. By this means the turbulent fluctuations associated with the transfer process are increased, thus setting up a scene favorable for turbulent-like mixing. In natural boundary layer it is difficult to study these structures because of their small sizes. In wake of the tab, these structures are magnified to a larger scale so that their dynamics and role in production, transport (of mass, momentum and energy) can be conveniently studied. Since the hierarchical hairpin-like structures are found to be responsible for sustaining turbulence in the boundary layer, it would be useful to study the topology and dynamics of these structures in detail, not only to understand the mixing enhancement process behind the tab but also to understand the turbulence phenomenon itself. The organized shedding of these vortical structures from the tab could be treated as a "model" experiment to provide insight into the natural turbulent boundary layer. Based on this objective, Yang et al. (1998) used PIV to

study the generation, evolution and regeneration of hairpin structures in the wake of the mixing tab.

Yang et al. (1998) analyzed more than 600 instantaneous velocity fields along streamwise wall-normal and streamwise spanwise planes to examine the vortex dynamics. They observed that the interaction between the low-speed boundary layer and the high-speed outer layer fluid is weaker in the near-tab region and stronger as the hairpin structures grow along the downstream. At a downstream distance of 20 tab heights, the hairpin structures were observed to lose their identity completely and there was no large-scale exchange of fluid between boundary and outer layers. The lifting angle of the hairpin structures was observed to be much smaller ($\approx 7^\circ$) than the value observed in natural boundary layers ($\approx 30^\circ$). Along with the primary hairpin structures, secondary hairpins were also noticed in the wake of the tab. Also a new type of offspring vortex structures with positive vorticity (i.e. reversed rotation compared to normal hairpins) was identified just below the primary hairpins.

Although both CVP and hairpin structures were confirmed to be present in the tab wake, in their studies Gretta and Smith (1993) as well as Yang et al. (1998) were not able to differentiate between the roles of these structures in mixing enhancement. If both structures co-exist in the tab flow everywhere, as indicated by Gretta and Smith (1993) (Fig. 1), then this flow cannot be used for producing pure hairpin structures as a "model" experiment. It is also not clearly understood how far these structures are active in the flow. Moreover, the hydrogen bubble technique Gretta and Smith (1993) used for visualization did not provide details of the structures, as this technique traces the outer edges of the structures only. On the other hand, the PIV measurements carried out by Yang et al. (1998) provided a series of instantaneous velocity-field snapshots in planes containing the streamwise direction, which do not lend themselves to a full grasp of the dynamics of the flow and the structure of CVP.

Even though the HEV mixer is accepted as an effective device in performing mixing, its flow dynamics is not understood. More details are necessary not only to estimate the mixing efficiency at different locations but also to modify the existing design for better performance. To meet the requirements and get a clearer picture about the flow behind the mixing tab, detailed flow visualization using the planar laser-induced flourescence (PLIF) technique is carried out in the present study. Unlike the hydrogen bubble technique, the PLIF technique, if properly adopted, can provide much more insight into the detailed physics of the flow. By observing the flow at various planes, it should be possible to investigate the dynamics of the individual structures. Hence, the main goal of the present study is to identify the different structures that emerge behind the mixing tab and their role in the mixing enhancement in various regions of the flow. To minimize the Schmidt number effect (Falco, 1977; Wallace et al., 1983; Wallace, 1984), the injection locations of the flourescence dye are carefully selected in such a way that they are reasonably close to the tab.

2. Experimental setup

The experiments are conducted in a closed circuit water tunnel made of Plexiglas. The test section has a dimension of 155 mm $\times$ 180 mm $\times$ 420 mm ($W \times D \times L$), and the flow is driven horizontally by a 0.5 hp pump. The top of the test section is closed with a removable cover so that the tunnel can be operated with a free surface (present experiments are conducted with closed top). A perforated cylinder distributes the flow uniformly into the horizontal section, reducing the possibilities

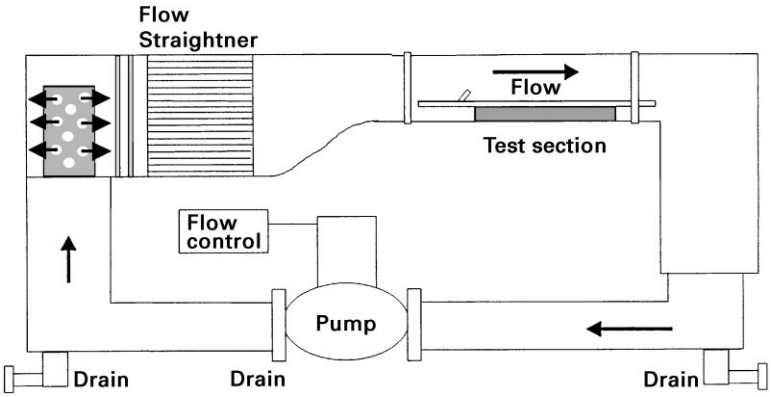

Fig. 2. Schematic of the water tunnel facility.

of trapping air bubbles in the flow. The uniformity of the flow in the test section is achieved by a combination of flow-straighteners (uniformly stacked plastic straws) and stainless-steel wire meshes before the contraction (Fig. 2). The flow velocity is controlled accurately with a frequency controller, which regulates the velocity by varying the rpm of the pump. The freestream velocity is maintained and the variation in the velocity is less than 0.5% during each experiment (typically about an hour). The freestream turbulence intensity is about 1% and pressure gradient is negligibly small ($U\ \mathrm{d}U/\mathrm{d}x = 2 \times 10^{-5}\ \mathrm{ms}^{-2}$ for $U \approx 0.18$ m/s).

A 10 mm thick, Plexiglas flat plate (600 mm (L) and 135 mm (W)) with an elliptical leading edge is mounted in the test section. The purpose of adopting the elliptical leading edge is to avoid flow separation at sharp corners. An aluminum block of 50 mm height supports the flat plate to avoid any interference by the wall (Fig. 3a). A tab, made of Plexiglas with an inclination angle $\alpha = 24.5^{\circ}$ and length $= 32$ mm (Fig. 3b), is mounted over the flat plate at a distance of 255 mm from the leading edge of the flat plate. The laminar boundary layer thickness at this location (upstream of the tab) is about 6.4 mm ($\sim$ 0.3 h). For flow visualization the dye is injected through a slit (DS1, Fig. 3a) with a 0.5 mm opening (70 mm wide in spanwise direction) machined carefully on the flat plate at a distance of 165 mm from the leading edge of the flat plate. The slit is machined at a shallow angle so as to avoid any disturbance on the development of the boundary layer by the dye injection. Additional dye injections slots (0.25 mm opening) are also machined along the edges of the tab (DS2, Fig. 3) in order to visualize the structures emerging from the tab more clearly. The dye reservoir is placed above the water tunnel and the flow rate is controlled carefully with three control valves. Coordinates x, y and z are streamwise, wall-normal, and spanwise directions respectively. In the present experiment all the distance measurement is calculated from the trailing edge of the tab. The distance is normalized by the tab height, h, from the wall (Fig. 3).

For the flow visualization mild solutions of laser-sensitive rhodamin 6G and sodium flourescien (1 mg/l of water) are used. Since the peak emission wavelengths of Rhodamin and sodium flourescein dyes are different (560 and 540 nm), by injecting them at appropriate locations, it is possible to separately differentiate the low-speed fluid of the boundary layer from high-speed fluid over the tab. The dye is illuminated using a 0.4 mm thick laser light sheet from a 4 W Ar-Ion laser (working wavelength 514.5 nm) with a combination of spherical and cylindrical lenses. The light sheet

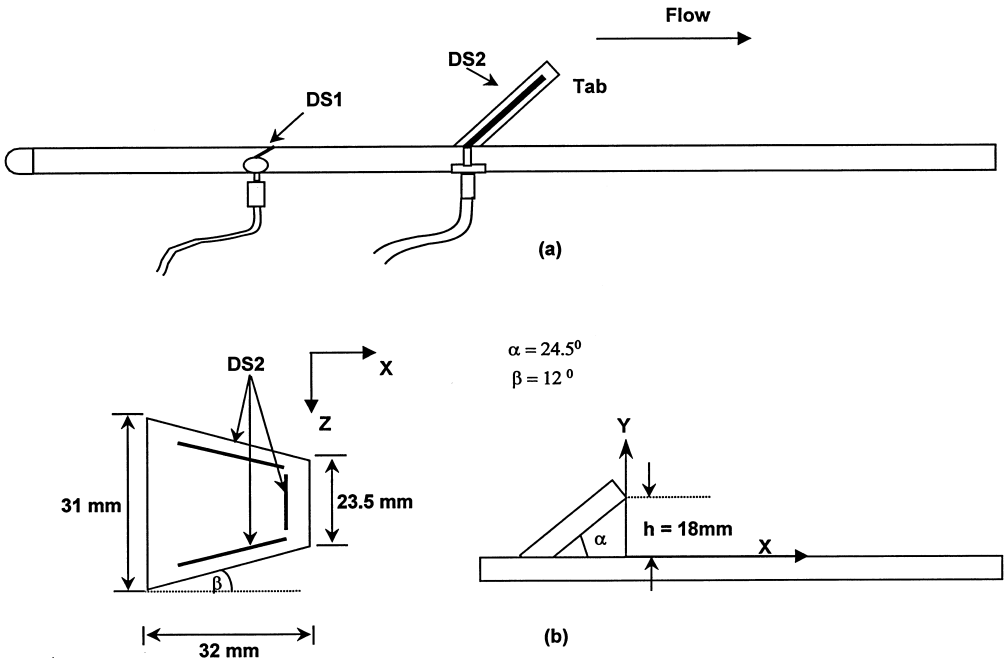

Fig. 3. Geometry of the tab and dye injection slots: (a) location of the dye injection slots, (b) tab geometry and size.

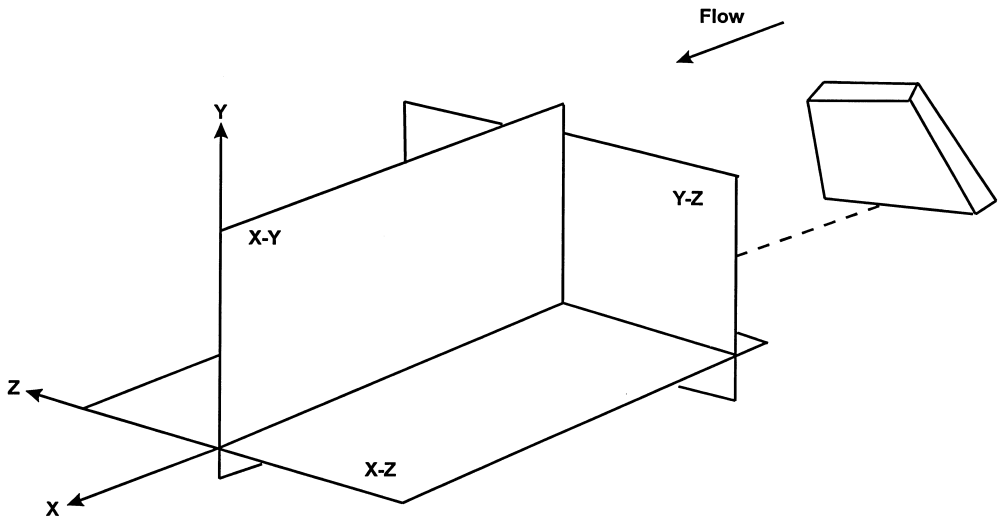

Fig. 4. Geometry of light sheet orientations.

orientation can be adjusted in all three planes of view (x–y, y–z and x–z planes – Fig. 4). The images are recorded using a CCD video camera (30 fps) and stored on VHS videotape for further analysis.

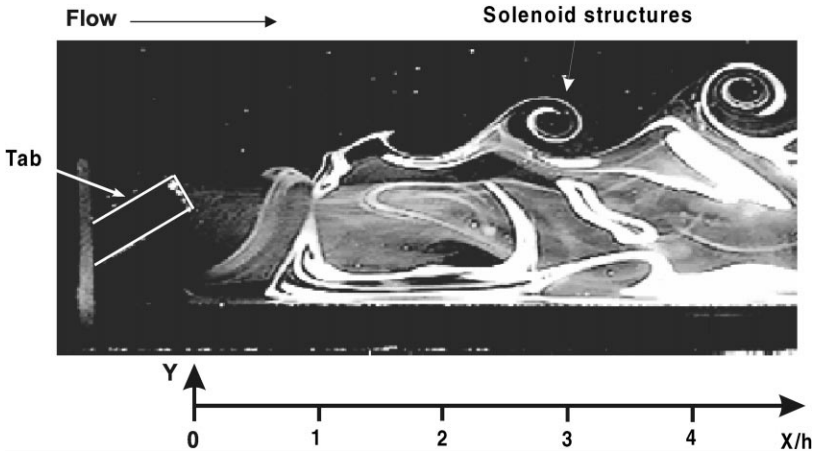

Fig. 5. Cross-section of the tab wake along x–y plane visualized by light sheet, showing development of the solenoid structures, which form the head of hairpin vortices.

3. Results

The experiments are conducted at different Reynolds number, R_h (based on the tab height, h and the freestream velocity, U) ranging from 450 to 2100. In general, the flow structures appear to have similar characteristic features over this Reynolds number range. Most of the flow visualization pictures presented in the paper are taken at $R_h = 700$ unless otherwise specified.

According to Gretta and Smith's (1993) conceptual model illustrated in Fig. 1, two distinctive flow structures, namely a counter-rotating vortex pair and a hairpin vortex array, co-exist all along the wake of the tab. This gives an impression that both structures are responsible for enhancement of mixing simultaneously all along the wake of the tab. To check the validity of this idea, the flow is viewed at various planes by orienting the laser light sheet properly so that each structure can be visualized intuitively.

Initially, the light sheet is oriented along centerline (line of symmetry) of the x–y plane and the Rhodamin dye is injected through the slots on the tab (DS2). The flow is viewed perpendicularly to the light sheet. Fig. 5 is a visualization of the development of the initial shear layer from the upper edge of the tab. The initial instability in the shear layer develops in the region $x/h < 0.5$, and the interface between the free-stream and the flow below the tab rolls up and forms a solenoid structure. This vortex structure while convecting downstream takes the shape of a hairpin with its legs extending possibly to the wall. The x–y cross section of these structures, as shown in Fig. 5, is similar to those observed in natural boundary layers (Praturi and Brodkey, 1978; Acalar and Smith, 1987a,b; Zhou et al., 1997).

Further experiments are conducted by injecting the dye (sodium flourescein) from the slot DS1 alone, located upstream of the tab. It is observed that the dye remain confined to the boundary layer until it reaches a particular location after the tab. At this location the dye appears to be acquiring some vertical velocity and is pumped up towards the upper layer. It then starts to trace the unsteady shear layer which is being developed by the tab trailing edge. Once enough dye is injected into the

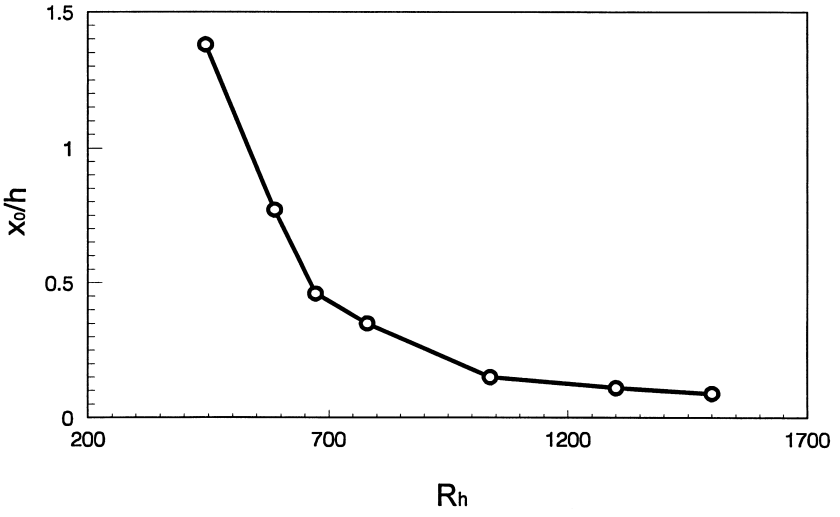

Fig. 6. Variation of initial pumping location x_0 with Reynolds number R_h.

outer layer, the signature of hairpin structures starts appearing as shown in Fig. 5. Irrespective of the dye injection location, the fully developed hairpin structures appear to form only when $x/h > 1.5$. This indicates that the hairpin structures, while still in the development stage, are not responsible for the cross stream mixing when $x/h < 1.5$. It is also observed that the initial pumping (i.e. the initial transport of low-speed fluid into outer layer) occurs at a certain location (referred to as x_0), which depends upon the Reynolds number. As the Reynolds number increases this location moves closer to the tab. For $R_h > 1700$, the initial pumping starts occurring immediately after the tab ($x_0/h \approx 0$). The variation of the initial pumping location x_0 with the Reynolds number is plotted in Fig. 6.

In order to understand more about the flow behavior in this near-wake region, the flow is viewed from the top while being illuminated with the light sheet oriented horizontal to the wall (x–z plane) at a height $y/h = 0.2$ from the flat plate. Fig. 7 shows the visualized cross section of the flow in this view. The immediately recognizable features in this picture are the legs of the hairpin structures that are located symmetrically on either sides of the tab centerline. These legs appear at $x/h = 1.5$ at the current height of visualization plane. The initial pumping location is indicated in Fig. 7. It is observed that this initial pumping point separates the recirculation zone behind the tab (like the recirculation zone behind any bluff body) from the tab wake. As the Reynolds number increases the size of the recirculation zone decreases and hence the initial pumping location moves towards the tab, as the plot in Fig. 6 shows.

Since the hairpin structures reach a fully developed stage only after a certain distance from the tab ($x/h > 1.5$), it is unlikely that they contribute to overall mixing in the near-wake region $x/h < 1.5$. However, the low-speed fluid is observed to be pumped into the high-speed region even before the hairpins are formed. Hence, it is obvious that the other large-scale structure in the flow, the counter-rotating vortex pair, is playing a major role in this region. To confirm this idea the flow is studied in the y–z plane. The light sheet is oriented along this plane at $x/h = 0.23$ from the tab trailing edge and the flow is viewed from downstream. Initially the Rhodamin dye (giving orange

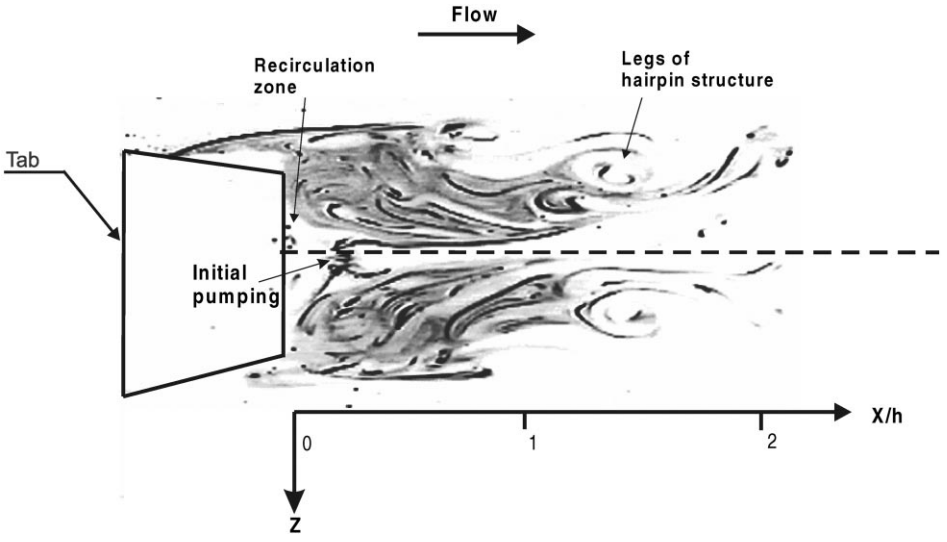

Fig. 7. Tab wake viewed in horizontal x–z plane. Light sheet is at $y/h = 0.2$. Contrast of picture reversed for better visual clarity.

fluorescence) is injected from the slots machined over the tab (DS2). The pressure difference between the upper and lower surfaces of the tab causes the fluid to roll up and initiates the spiraling motion (Gretta and Smith 1993). This leads to the counter rotation of the fluid. Fig. 8(a)–(d) shows the initial stage of the CVP at different Reynolds numbers. Although the gap between the counter-rotating vortices decreases with increasing Reynolds number (the gap becomes virtually indiscernible for $R_h > 1300$), there is always an upward pumping of surface low-speed fluid along the centerline in the gap. To differentiate the low- and high-speed fluids in the flow, sodium flourescein dye (giving green fluorescence) is also released slowly from the near wall slot (DS1). The green-color dye remains confined near the wall until it reaches the edge of the recirculation zone ($x/h = 0.2$) as can be seen in Fig. 5. Once the dye reaches this region, the action of the counter-rotating vortex pair at the plane of symmetry induces a pumping action, which transports this green low-speed near-wall fluid into the outer shear layer and initiates the mixing process. This upward motion is marked by arrows in Fig. 8. After reaching the top, the low-speed fluid, marked by the green dye, is entrained into the counter-rotating vortices. While convecting downstream, the dye remains confined inside the structure and undergos a thorough mixing.

Although the two large vortices rotate continuously, the pumping of the green near-wall dye into the outer shear layer by the CVP is observed to occur in the form of pulses (at locations marked in Fig. 8). This seems to suggest that, even though the migration of low-speed fluid into high-speed region is induced by the counter-rotating vortices, the onset of the initial pumping may be responding to the instabilities being developed on the outer shear layer. This can be checked by observing the thin layer of dye at the top, where the outer shear layer lies. Each time there is a strong pulsing in the outer shear layer, a bulk of low-speed green dye is seen pumped upward.

The frequency of this pumping by CVP, a function of Reynolds number, is different from the hairpin vortex-shedding frequency, which is observed further downstream (when the hairpins are

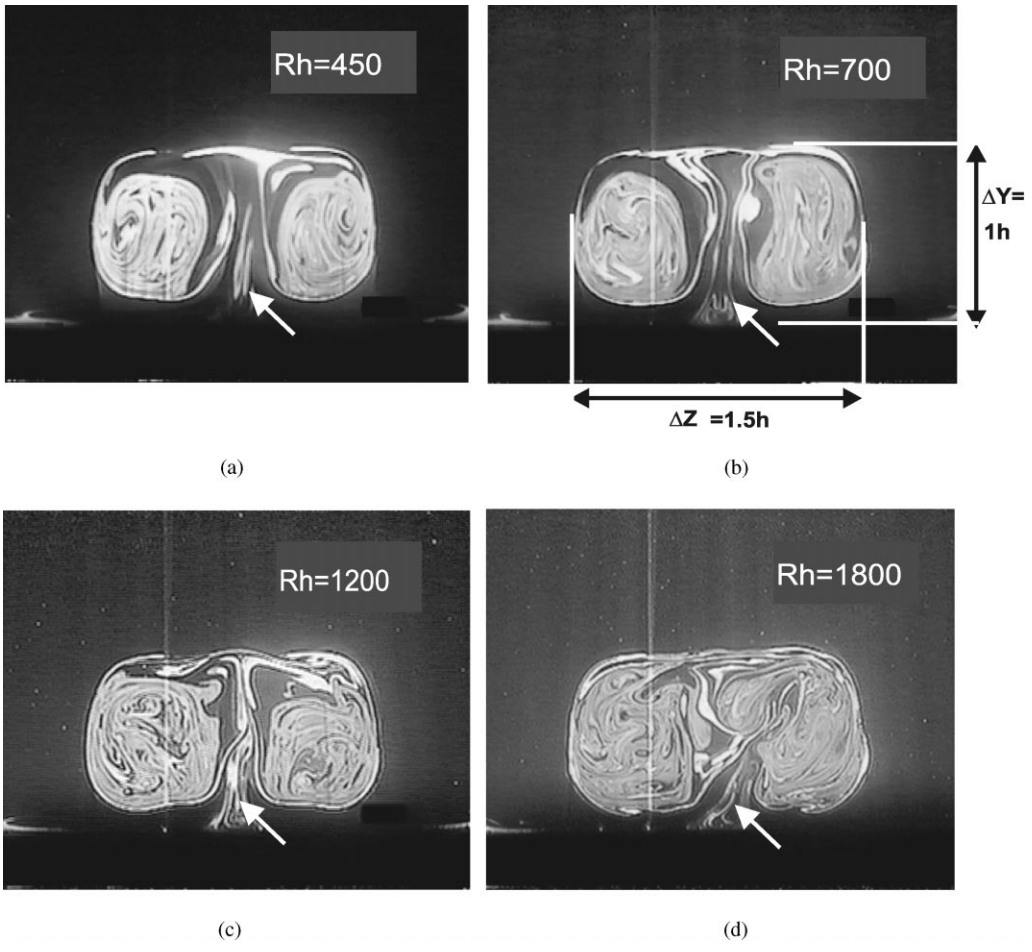

Fig. 8. Counter-rotating vortex pair in the near-wake region. The light sheet is orientated along y–z plane at $x/h = 0.2$. The arrows point to the upward motion of the boundary layer fluid: (a) $R_h = 450$, (b) $R_h = 700$, (c) $Rh = 1200$, (d) $R_h = 1800$.

fully developed). In order to quantify this observation, the hairpin vortex shedding frequency is measured at $x/h = 2$ by recording the flow along x–y plane and ensemble averaging more than 600 frames at each Reynolds number in the following procedure. Over 600 frames of the flow visualization video (in x–y plane) are analyzed for this purpose. In each frame the hairpin structures are identified (if present) by fixing conditions such as the size (reference to the tab height), location (counted only if they occur between the specified locations). In this way the uncertainty involved in counting stray vortices can be eliminated. This routine is repeated for 5 sets of video clips (600 frames each) and the mean of the five sets is calculated and used for final analysis. The variation among the data is about 2% only. Similarly the pumping frequency of CVP is measured at $x/h = 1$, from the view in y–z plane, by observing the upward flow (traced by green dye) induced by the counter-rotating vortex pair. Fig. 9 shows the measured hairpin vortex shedding frequency f_s (triangles) and CVP pumping frequency f_p (squares) as functions of Reynolds number. As expected,

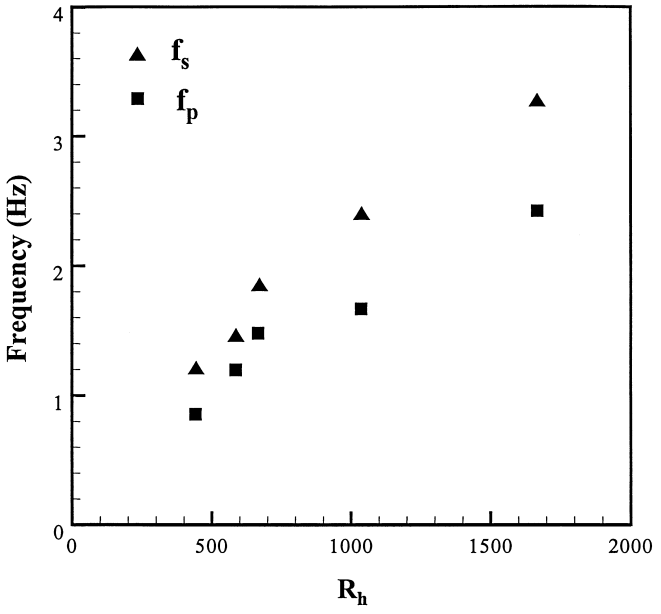

Fig. 9. Measured hairpin vortex shedding frequency f_s (triangles) and initial CVP pumping frequency f_p (squares) as functions of Reynolds number.

both frequencies increase with Reynolds number, but the corresponding Strouhal numbers (fh/U, where f is frequency, h the tab height and U the freestream velocity) decrease slightly over this range. At $R_h = 700$ (the condition for most of the experimental observations in the current work), the Strouhal numbers corresponding to hairpin shedding f_s and CVP pumping f_p are 0.84 and 0.69, respectively. It is evident from the plot that the hairpin vortex-shedding frequency is higher than the CVP pumping frequency. It should be noted that the two frequencies are measured at different locations (pumping frequency at $x/h = 1$ and hairpin shedding frequency at $x/h = 2$), where the structures are individually prominent.

After confirming the presence and the role of the counter-rotating vortex pair in the near-wake region, the next step is to determine the extent over which it dominates the flow. For this purpose the observations are continued at $R_h = 700$ by traversing the light sheet in y–z plane along the streamwise direction (x). During this procedure, it is observed that when the light sheet is in the region $x/h = 1.2$–1.5, both counter-rotating and hairpin structures exist together, almost with equal strength (Fig. 10). Although their individual contributions to bringing near-wall fluid up are not clear, it can be postulated that both are responsible in this region of the flow. As the light sheet is traversed further downstream (pictures not shown), beyond $x/h = 1.5$ the counter-rotating vortices slowly lose their strength while the hairpins start gaining strength and dominate the flow. The observations show that the complete transition occurs somewhere in the region $1.2 < x/h < 2$. In the region $x/h > 2$ hairpin structures alone are present in the flow.

To show the dynamics of a hairpin vortex in the region $x/h > 2$, a time sequence of a passing hairpin structure through a light sheet (y–z plane) at $x/h = 6$ is shown in Fig. 11(a)–(h). These figures show no evidence of the presence of CVP, and the flow is completely dominated by large,

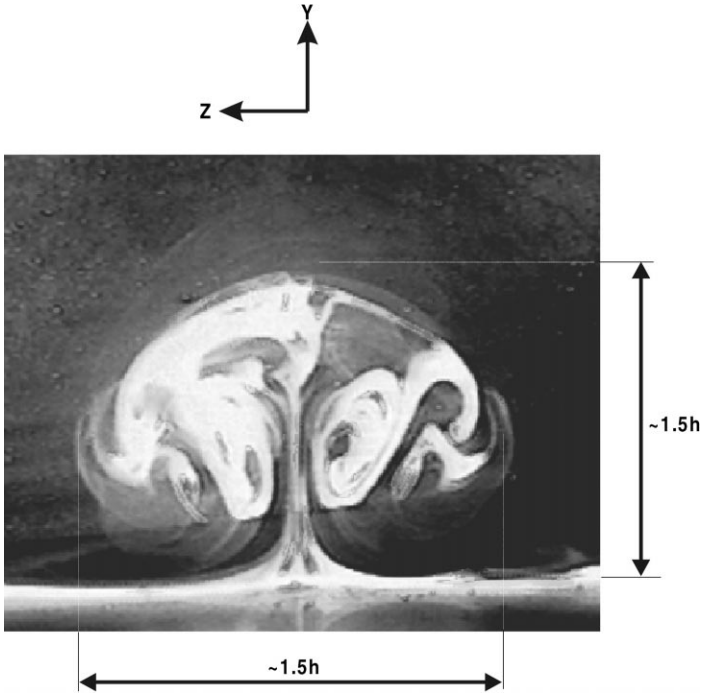

Fig. 10. View in y–z plane at $x/h = 1.2$. Both counter-rotating and hairpin structures are present.

fully developed hairpin structures. In (a), the pair of legs of a hairpin vortex, which has just passed the light sheet, is present like a mushroom. It can be observed from the figure that these legs, while passing the plane of view, interact with the near-wall fluid and pump it to the outer shear layer. While the migration of the low-speed fluid into the high-speed region is taking place, the next hairpin structure starts following the previous one (Fig. 11(b)–(h). The head of the following hairpin structure appears right above the legs of the preceding structure. The vortex passing frequency is calculated by counting more than 500 hairpin structures past the light sheet at this location. It is found that the hairpin vortex passing frequency (and hence the pumping by hairpin legs) is approximately equal to the hairpin shedding frequency, measured from the side view (x–y plane) for all the Reynolds numbers tested. This implies that the pumping of fluid from surface to outer layer by hairpin vortices occurs at the same rate as the hairpin vortex shedding.

The transition from CVP to hairpins indicates that except for a small region, the two prominent structures in the flow contribute to mixing separately. As discussed above (Fig. 9), pumping by CVP (in the near wake) occurs at a lower frequency than pumping by hairpin legs (further downstream). This may suggests that cross-stream mixing by CVP is weaker than by hairpin vortices.

To find the distance up to which the hairpins structures sustain their identity, the light sheet is traversed further downstream. The size of the hairpins vary almost linearly with distance up to $x/h = 10$, and beyond this region they start losing their strength and shape. These structures traced by flourescence dye are no longer present in the flow visualization in the range $x/h > 15$. However, the real vortex structures could actually exist even further downstream. A modified view of the flow structures and their dominant regions are sketched in the Fig. 12. Since hairpin vortices clearly

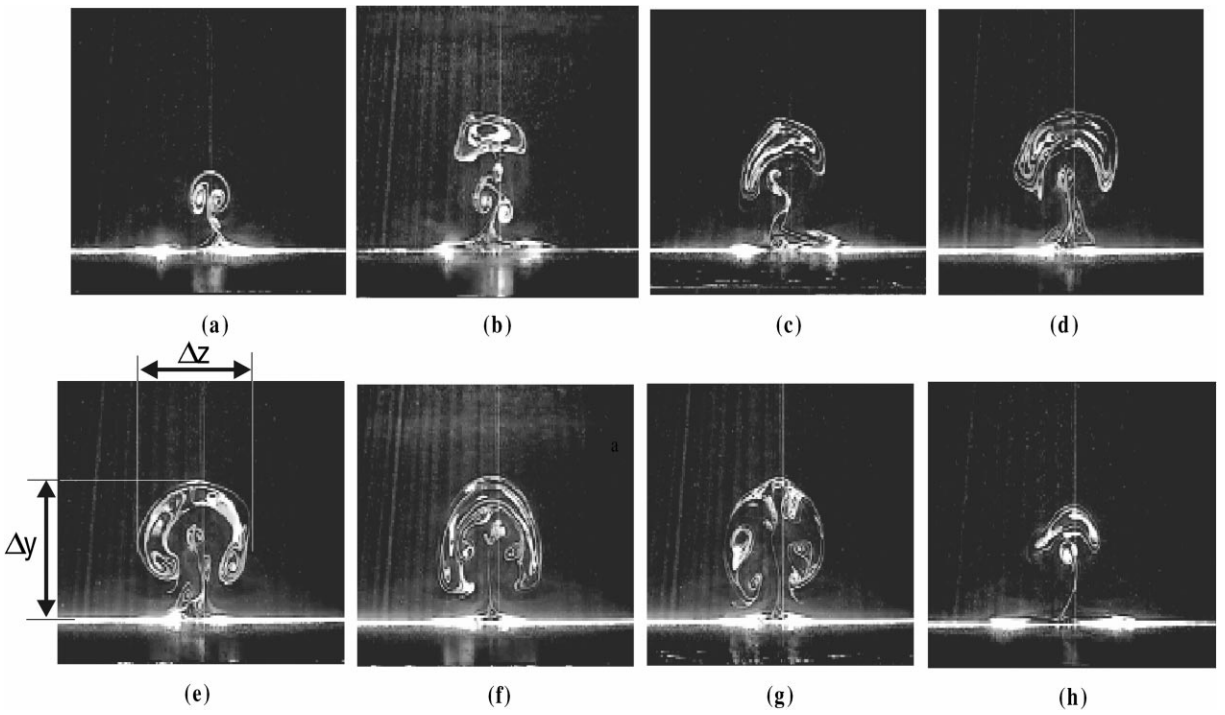

Fig. 11. Hairpin vortex passage in the y–z plane located at $x/h = 6$. (a)-(h) are snap shots for a complete cycle of 0.5 sc. The typical height of the vortex Δy is $5h$ and typical width Δz is $3h$.

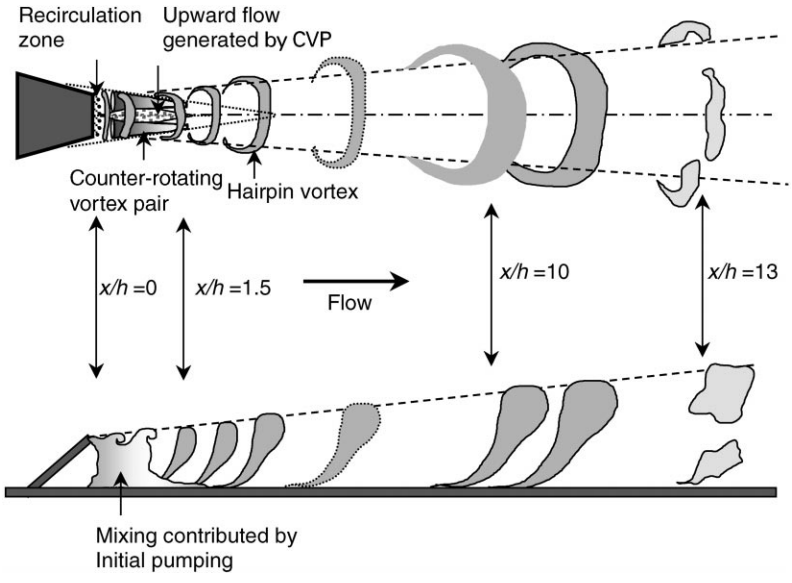

Fig. 12. Illustration of the coherent structures that evolve in the wake of the mixing tab. The schematic is drawn based on the present flow visualization observation.

persist for a much longer downstream distance than the CVP, they play a much more prominent role in enhancing mixing in the tab wake.

4. Conclusion

Flow visualization experiments at R_h (Reynolds number based on the tab height) are conducted behind the wake of a surface-mounted, passive mixing tab to understand the role of individual coherent structures that dominate the flow. It is observed that the two principal flow structures, counter-rotating vortex pair and hairpin vortices, dominate different regions of the flow. This is in contrary to Gretta and Smith's (1993) illustration where both structures co-exist all along the wake. A counter-rotating vortex pair, formed by the pressure difference that exists on the top and bottom of the tab, dominates the flow in the near-wake region ($x/h < 1.5$) immediately after the recirculation zone. These counter-rotating vortices, while convecting along the downstream, transport the low-speed surface fluid into the high-speed outer layer by means of a pumping action. Beyond this region ($x/h > 1.5$) these vortices lose their strength, and hairpin structures start dominating the flow. Up to $x/h = 10$ the hairpin vortices sustain their shape and energy, and beyond this region they start loosing their shape and size. Their identity is completely lost after $x/h = 15$. The transition from CVP to hairpins indicates that except for a small region, the two prominent structures in the flow contribute to mixing separately. Furthermore, pumping of low-speed surface fluid by CVP occurs at a lower frequency than pumping by hairpin vortex legs. This may suggest that cross-stream mixing by CVP is weaker than by hairpin vortices.

Acknowledgements

The authors wish to thank Vishal Khosla for his contribution in the completion of this manuscript and his helpful experiments. They also acknowledge stimulating discussions with Wenming Yang and Jian Sheng. This work is supported by NSF grant CTS-9625307.

References

Acalar, M.S., Smith, C.R., 1987a. A study of hairpin vortices in a laminar boundary layer. Part 1. Hairpin vortices generated by a hemisphere protuberance. J. Fluid Mech. 175, 1–42.

Acalar, M.S., Smith, C.R., 1987b. A study of hairpin vortices in a laminar boundary layer. Part 2. Hairpin vortices generated by a fluid injection. J. Fluid Mech. 175, 43–85.

Asai, M., Nishioka, M., 1995. Boundary layer transition triggered by hairpin eddies at subcritical Reynolds numbers. J. Fluid Mech. 297, 101–122.

Corino, E.R., Brodkey, R.S., 1969. A visual investigation of the wall region in turbulent flow. J. Fluid Mech. 37, 1–36.

Falco, R.E., 1977. Coherent motions in the outer region of turbulent boundary layers. Phy. Fluids 20, s124–32.

Gretta, W.J., 1990. An experimental study of the fluid mixing effects and flow structure due to a surface mounted passive vortex generating device. M.S. Thesis, Lehigh University, Bethlehem, PA.

Gretta, W.J., Smith, C.R., 1993. The flow structure and statistics of a passive mixing tab. J. Fluid Eng. 115, 255–263.

Hama, F.R., Long, J.D., Hegarty, J.C., 1957. On transition from laminar to turbulent flow. J. App. Phys. 28, 388.

Harnby, N., Edward, M.F., Nienow, A.W. (Eds.), 1985. Mixing in the Process Industries. Butterworth, London.

Head, M.R., Bandyopadhyay, P., 1981. New aspects of turbulent boundary layer structure. J. Fluid Mech. 107, 297–337.

Kim, H.T., Kline, S.J., Reynolds, W.C., 1971. The production of turbulence near a smooth wall in a turbulent boundary layer. J. Fluid Mech. 50, 133–160.

Kline, S.J., Runstadler, P.W., 1959. Some preliminary results of visual studies of the flow model of the wall layers of the turbulent boundary layer. Trans. ASME, Ser. E 2, 166–170.

Kline, S.J., Reynolds, W.C., Schraub, F.A., Runstadler, P.W., 1967. The structure of turbulent boundary layers. J. Fluid Mech. 30, 741–773.

Lin, J.C., Howard, F.G., 1989. Turbulent flow separation control through passive techniques. AIAA paper no. AIAA-89-0976.

Nishioka, M., Asai, M., Iida, S., 1981. Wall phenomena in the final stage of transition to turbulence. In: Meyer, R.E. (Ed.), Transition and Turbulence. Academic Press, New York, pp. 113–126.

Nishioka, M., Asai, M., 1984. Evolution of Tollmien-Schlichting waves into wall turbulence. In: Tatsumi, T. (Ed.), Turbulence and Chaotic Phenomena in Fluids. North-Holland, Amsterdam, pp. 87–92.

Panton, R.L., 1999. Self-sustaining mechanism of wall turbulence – a review. Paper No. AIAA 99-552.

Peridier, V.J, Smith, F.T., Walker, J.D.A., 1991. Vortex induced boundary layer separation. Part 2. Unsteady interaction boundary layer theory. J. Fluid Mech. 232, 133–165.

Praturi, A.K, Brodkey, R.S., 1978. A stereoscopic visual study of coherent structures in turbulent shear flow. J. Fluid Mech. 89, 251–272.

Robinson, S.K., 1991. Coherent motion in turbulent boundary layers. Ann. Rev. Fluid Mech. 23, 601–639.

Runstadler, P.G., Kline, S.J., Reynolds, W.C., 1963. An experimental investigation of flow structure of the turbulent boundary layer. Report No. MD-8, Department of Mechanical Engineering. Stanford University, Stanford, California.

Smith, C.R., Metzler, S.P., 1983. The characteristics of low-speed streaks in the near-wall region of a turbulent boundary layer. J. Fluid Mech. 129, 27–54.

Smith, C.R., Schwartz, S.P., 1983. Observation of streamwise rotation in the near-wall region of a turbulent boundary layer. Phy. Fluids 26, 641–652.

Smith, C.R., Walker, J.D.A., Haidari, A.H., Sobrun, U., 1991. On the dynamics of near-wall turbulence, Philos. Trans. Roy. Soc. Lond. A. 336, 131–175.

Stevens, A.V., Collins, G.A., 1955. Turbulent boundary layer control by ramps and wedges. Australian Aeronautical Research Commission Report No. ACA-55.

Theodorsen, T., 1952. Mechanism of turbulence. In: Proceedings of seconnd Midwestern Conference on Fluid Mechanics, Ohio State University, Columbus, OH.

Wallace, J.M., Balint, J.J, Mariaux, J.L., Morel, R., 1983. In: Chen, W.F., Leuis, A.D.M. (Eds.), Recent Advances in Engineering Mechanics and their Impact on Civil Engineering Practice. Purdue University, pp. 1198–1201.

Wallace, J.M., 1984. In: Tatsumi, T. (Ed.), Turbulence and Chaotic Phenomena in Fluid. North-Holland, Amsterdam, pp. 447–452.

Yang, W., Sheng, J., Meng, H., 1998. Study of hairpin vortex dynamics and turbulence statistics of a surface-mounted mixing tab wake using PIV. The ninth International Symposium for Applications of Laser Techniques to Fluid Mechanics, Lisbon, Portugal, July 13-16, 1998.

Zhou, J., Meinhart, C.D., Balachandar, S., Adrain, R.J., 1997. Formation of coherent hairpin packets in wall turbulence. TAM Report no. 845. UILU-ENG-97-6006, University of Illinois.